INTERNATIONAL JOURNAL FOR NUMERICAL METHODS IN FLUIDS, VOL. 18, 1185–1209 (1994)

FINITE ELEMENT FORMULATIONS FOR LARGE-SCALE, COUPLED FLOWS IN ADJACENT POROUS AND OPEN FLUID DOMAINS

A. G. SALINGER, R. ARIS AND J. J. DERBY

Department of Chemical Engineering and Materials Science, University of Minnesota, Minneapolis, MN 55455, U.S.A.

SUMMARY

Two approaches which employ the finite element method to solve for large-scale, coupled, incompressible flows through adjacent porous and open domains are developed and evaluated in a model for the spontaneous ignition of coal stockpiles. Both formulations employ the Navier–Stokes equations do describe flow in the open region; two different descriptions, Darcy's law and the Brinkman equation, are employed to model flows within the porous region. The formulation which uses Darcy's law employs the Beavers–Joseph slip condition and a novel implementation of the interfacial conditions. The other approach invokes the Brinkman equation: this considerably simplifies the implementation of matching conditions at the interface between the porous and open fluid domains, but also results in velocity boundary layers in the porous region adjacent to this interface which can be difficult to resolve numerically. A direct comparison of model results shows that the Darcy–slip formulation produces solutions which are more accurate and more economical to compute than those obtained using the Brinkman formulation.

1. INTRODUCTION

There is a vast body of research dealing with the mathematical modelling of flows through porous media. The modelling of coupled flows through adjacent porous and open domains has received much less attention; nevertheless, these porous/open flows occur in many interesting and important systems. Examples of engineering applications include porous bearings,[1–3] the mushy zone in alloy solidification[4–7] and heat transfer in walls with fibrous insulation.[8,9] Bio-engineering systems include the lubrication of human and artificial joints and blood flow in lungs and arteries.[10] Flow through fractured porous media also involves the coupling between open and porous regions; examples include the flow of water, oil or magma through geological media.[11–14] Excellent overviews of prior research on porous/open flows have been presented by Tien and Hong,[15] Rudraiah[16] and Prasad.[17]

Our investigation into the methodologies employed for solving this class of problems was motivated by the study of the spontaneous combustion of coal stockpiles.[18] Piles of coal being transported to or stored at utility plants react exothermically with oxygen and can ignite, which is both dangerous and costly. Buoyancy-driven convection is an important factor in setting the ignition conditions by transporting oxygen into the pile and simultaneously transporting heat away. Our study of this system[18] was the first to include a self-consistent description of the coupled chemical reaction, mass transport and natural convective flows both within the stockpile (modelled as a porous medium) and in the air surrounding the pile. Herein we address the issues

CCC 0271–2091/94/121185–25

Received 27 July 1993
Revised 20 December 1993

involved with the formulation and numerical solution of such coupled flows in porous/open fluid systems.

The first issue which arises in the formulation of a mixed porous/open flow problem is the proper mathematical form of the governing equations in each region. The flow of an incompressible fluid in a homogenous domain is well represented by the Navier–Stokes equations; however, there are several possible choices for describing flow in a porous domain. The two most commonly used equations for flows in porous media are Darcy's law and Brinkman's equation. We shall outline some of the features of these equations below, followed by a brief discussion of their prior application to describe porous/open fluid flows.

Well over a century ago Darcy[19] presented an empirical model which stated that the superficial velocity of a fluid in a saturated porous medium is related linearly to the pressure gradient in the medium. With the inclusion of the body force term, Darcy's law takes the form

$$\nabla \tilde{P} = -\frac{\mu}{\kappa} \tilde{v} + \rho \mathbf{g}, \tag{1}$$

where $\tilde{P}$ is the pressure, $\tilde{\mathbf{v}}$ is the volume-averaged fluid velocity, μ is the viscosity, κ is the permeability of the porous medium, ρ is the fluid density and $\mathbf{g}$ is the gravity vector. In 1947 Brinkman[20] pointed out that Darcy's law does not include a term to account for the viscous interaction among fluid particles, so that it cannot represent boundary layers such as those which arise near an impermeable wall or a faster-moving fluid. To overcome this apparent deficiency, Brinkman presented the following modified relation which includes a viscous force term taken from the Stokes equation as well as those terms present in Darcy's original equation:

$$\nabla \tilde{P} = -\frac{\mu}{\kappa} \tilde{\mathbf{v}} + \mu' \nabla^2 \tilde{\mathbf{v}} + \rho \mathbf{g}, \tag{2}$$

where μ' is an effective viscosity which is a function of the fluid viscosity and the characteristics of the porous medium.

There has been a long and ongoing debate regarding the appropriateness of Darcy's law versus the Brinkman equation. Certainly Darcy's law is correct for one-dimensional and slowly spatially varying flows. The ability of Darcy's law to describe experimental measurements of flows through porous media has been demonstrated for an extensive variety of viscous liquids at low Reynolds numbers.[21–23] In addition, Irmay[24] has shown that Darcy's law can be derived theoretically by spatially averaging the Navier–Stokes equations in a random porous medium in the limit of low Reynolds number. However, Darcy's law does not hold in all situations; modifications have been suggested by Forchheimer,[25] Ergun,[26] Vafai and Tien[27] and Joseph *et al.*[28] as well as by Brinkman. The validity of the Brinkman equation has been rigorously verified in the limit of very low volume fraction of solids, i.e. porosities very near unity,[29–34] and many studies have addressed the proper choice for the effective viscosity μ'.[20,31–36] However, many researchers have pointed out that the Brinkman equation is not rigorously correct in situations where the volume fraction of solids is significant,[31,33,37] which is often the case for a typical porous medium.

The choice of employing Darcy's law or the Brinkman equation for the porous domain in a porous/open fluid problem involves not only the fundamental issues of appropriateness discussed above but also issues which arise in linking the flows across the interface between the two domains. Since only a first-order derivative of the pressure is present in Darcy's law, equation (1), the complete specification of all velocity components is not possible along the boundaries of the porous region; this poses special problems when attempting to match conditions in an adjacent open domain, where conditions for all velocity components must be specified for the

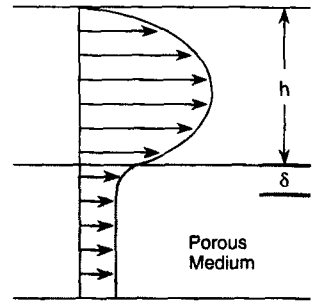

Figure 1. The flow of fluid in an open channel overlying a saturated porous medium. A boundary layer of thickness δ connects the flow of the open fluid region to the flow within the porous medium. After Beavers and Joseph[38]

Navier–Stokes equations. To address these issues, Beavers and Joseph[38] performed experiments measuring the mass efflux of Poiseuille flow over a permeable block and postulated that the flow field must take on a form similar to that shown in Figure 1. Arguing that Darcy's law would hold in the interior of the porous region but not necessarily near the boundary, Beavers and Joseph proposed that the interfacial velocities of the exterior fluid and the fluid within the porous region could be related by an *ad hoc* boundary condition which admits a discontinuity in the tangential component of flow. This condition was expressed as

$$\left(\frac{d\tilde{v}_x}{dy}\right)_o = \frac{\alpha}{\kappa^{1/2}}(\tilde{v}_{x,o} - \tilde{v}_{x,p}), \tag{3}$$

where the x-co-ordinate direction is taken to be parallel to the interface and the y-co-ordinate direction is perpendicular to the interface (see Figure 1). The subscript 'o' refers to the open fluid domain where the Navier–Stokes equations hold, the subscript 'p' refers to the porous medium in which Darcy's law holds, and α is a slip coefficient which depends only on the properties of the porous medium. Subsequent experimental investigations of porous/open fluid systems supported the ideas behind the Beavers–Joseph boundary condition.[39–41] Theoretical derivations and further modifications of this condition have also been presented which give equation (3) a more solid fundamental interpretation.[42–47]

Interestingly, although Beavers and Joseph were the first to propose such a relationship for adjacent flows between an open channel and a porous medium, the idea of fluid slip at solid boundaries has been proposed in many other contexts. Over 165 years ago Navier[48] formulated a slip condition in which a discontinuity in the tangential fluid velocity at a solid boundary was assumed to be proportional to the shear stress in the fluid. This approach has also been employed in modelling macroscopic flows in several other systems where the no-slip hypothesis yields unsatisfactory results. The infinite stress predicted as a result of the no-slip hypothesis applied at a moving contact line during coating flows has led to the use of slip conditions in some formulations.[49] Macroscopic slip phenomena have also been invoked to describe the flows of polymer fluids which exhibit complicated rheological behaviour.[50]

The use of the Brinkman equation (2) in a two-domain system poses no special difficulties, since the second-order derivative of velocity allows for the specification of continuous normal and tangential velocities as boundary conditions across the porous/open fluid interface. In addition, this implementation can be made to be consistent with the Darcy–slip formulation described above under some special conditions. Neale and Nader[45] have shown for the case of

flow in a channel bounded by a porous layer that the choice of the Beavers–Joseph slip coefficient as

$$\alpha = \left(\frac{\mu'}{\mu}\right)^{1/2} \tag{4}$$

will yield identical velocity profiles in the open fluid layer for both the Darcy and Brinkman formulations.

Buoyant, incompressible flows in a coupled porous/open fluid system provide the basis for our comparative study of the Darcy and Brinkman formulations; such flows have been modelled in the past using both these implementations (see Reference 17 for an extensive list of references). Nield[52] first studied the onset of natural convection in a system with an open fluid overlying a porous lium. In that study and a later one[37] Nield employed Darcy's law with the Beavers- seph boundary condition. Pillatsis *et al.*[53] and Taslim and Narusawa[54] also employed the Dar(ormulation to study the onset of convection in various configurations. The Brinkman formulation was employed by Somerton and Catton[55] to study natural convection in a fluid above a heat-generating, saturated porous medium. Poulikakos and Kazmierczak[9] also used the Brinkman formulation to study flow in a channel with a porous layer in both parallel plate and cylindrical geometries. Nishimura *et al.*[56] studied convection in a fluid overlying a saturated porous medium with the Brinkman equation. Beckerman *et al.*[57–59] performed extensive analyses of flow in square enclosures driven by an imposed horizontal temperature gradient. Song and Viskanta[60] continued this work for an anisotropic porous layer. The work presented in References 57–60 employed the Brinkman formulation.

Unfortunately, none of the above studies compared the performance of both the Darcy–slip and Brinkman formulations in the context of such problems. We endeavour to make this comparison here by solving the coal stockpile ignition problem[18] using finite element implementations of both approaches. We emphasize that we do not wish to advocate the use of Darcy's law or the Brinkman equation on the basis of fundamental correctness; rather we wish to address the implications of their use for the description of large-scale, coupled flows within porous and open fluid regions.

Before embarking on this comparison, it is useful to consider the physical and mathematical characteristics of flows near the interface between a porous and an open fluid region. Saffman[43] pointed out that the boundary layer within the porous medium, postulated originally by Beavers and Joseph,[38] should scale with the square root of the permeability of the medium, i.e. $\delta \sim \mathcal{O}(\kappa^{1/2})$. Neale and Nader[51] later solved for the thickness of the boundary layer in the specific configuration, depicted in Figure 1, of a porous region bounded by an open fluid channel. Here the boundary layer thickness δ is defined as the distance from the interface to the point where the velocity predicted by the Brinkman formulation is within 1% of the bulk or Darcy value. They found that in the case of channel flow with $\mu = \mu'$ the boundary layer thickness δ is dependent on the permeability κ and channel thickness h according to the relation

$$\delta = \kappa^{1/2} \ln\left[50\left(\frac{h}{\kappa^{1/2}} - 1\right)\right]. \tag{5}$$

Figure 2 shows this boundary layer thickness plotted as a function of the porosity ε for several different channel widths when the Kozeny–Carman relation[22] is employed to determine the permeability of the medium (i.e. $\kappa = D_p^2\varepsilon^3/150(1-\varepsilon)^2$, where D_p is the average particle diameter). The boundary layer thickness decreases dramatically with decreasing porosity and is less than a few particle diameters in width over a wide range of typical values for porosity. When

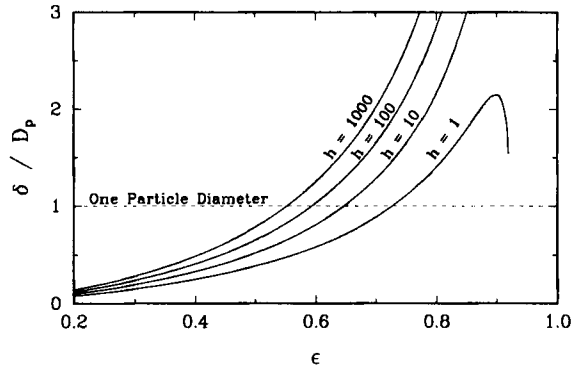

Figure 2. A plot of equation (5) shows that the porous boundary layer thickness δ is of the order of one particle diameter or smaller for a wide range of porosities ε and dimensionless channel widths h/D_p. For exterior flows the dimensionless channel width would correspond roughly to the thickness of the open fluid region boundary layer

the width of the boundary layer is comparable with or less than the average particle size of the porous medium, the averaging techniques used to derive the Darcy drag term in the Brinkman equation are not rigorously valid.[31,33,37] The accurate resolution of this boundary layer is a significant challenge for any numerical method, especially since the velocity gradients in these systems are typically very steep, with tangential velocities often decreasing by several orders of magnitude from values in the open region to those within the porous region. These challenges will be made clear in Section 4.2 by our numerical calculations.

Interestingly, the aspect of boundary layer resolution in the numerical solution of coupled porous/open flow problems using the Brinkman equation has received little attention. Nishimura *et al.*[56] employed the finite element method to solve for a streamfunction–vorticity formulation using Brinkman's equation and found that model results were very sensitive to the discretization in the porous medium near the porous/open fluid interface. Their solutions changed dramatically unless the element placed adjacent to the interface was at least as small as $\kappa^{1/2}$, which is consistent with the scaling of the boundary layer discussed above. This concern about boundary layer resolution is notably absent in virtually all other studies, although Poulikakos and Kazmierczak,[9] Beckerman *et al.*[57–59] and Song and Viskanta[60] employed *ad hoc* schemes to smooth the variation in physical properties between the open fluid and porous domains. Typical of this approach is the scheme of Beckerman *et al.*[57] which involved the application of a control volume discretization to a single equation written for both domains. This single equation contained a binary parameter which selectively chose the appropriate terms of the equation to yield the Navier–Stokes equation in the open domain and Brinkman's equation in the porous region. A harmonic mean formulation for the interface diffusion coefficients between two control volumes was also employed. Beckerman *et al.* claimed that this formulation automatically satisfied the matching conditions at the interface, since the algorithm ensured continuity of velocities and stresses at every point in the computational domain. In addition, the approach was promoted for its ease of implementation and its ability to avoid the need for an excessively fine grid at the porous/fluid layer interface.[57] Comparisons of predicted temperature fields by Beckerman *et al.*[58,59] agreed reasonably well with experimental data, yet the solution streamlines exhibited discontinuous slopes at the interface. This would indicate discontinuities in the computed tangential velocities, which would contradict the velocity continuity conditions meant to be satisfied at the interface.

From a purely algorithmic point of view the boundary layer produced by use of the Brinkman equation is a nuisance; its presence must be accommodated by mesh resolution or by the use of various solution-smoothing techniques such as those employed in the studies mentioned above. An advantage of the Darcy–slip formulation is that it does not give rise to this boundary layer and thus avoids the numerical difficulties associated with resolving it. Instead, the effects of this layer are accounted for through the slip condition of Beavers and Joseph.[38] We argue here that the Darcy–slip formulation is preferred over the Brinkman formulation because of this issue. As long as the characteristic length scales associated with the problem to be solved are much larger than the boundary layer in the porous region, the Darcy–slip formulation adequately and economically yields solutions for porous/open fluid problems.

We present our model problem and the two mathematical formulations in Section 2. In Section 3 we detail a novel finite element implementation of the Darcy–slip formulation and the numerical approach required for the Brinkman formulation. Results are put forth in Section 4. Further discussion on the strengths and weaknesses of the formulations will be presented in Section 5.

2. PROBLEM SPECIFICATION AND FORMULATION: THE SPONTANEOUS IGNITION OF A COAL STOCKPILE

We employ the coal stockpile ignition problem[18] as our model system for evaluating solution strategies for coupled flows within porous and open domains. In this problem the shape of the coal pile is assumed to be a frustrum surrounded by a homogeneous air region (see Figure 3(a)). The coal pile is considered to be an isotropic porous medium in which an exothermic oxidation

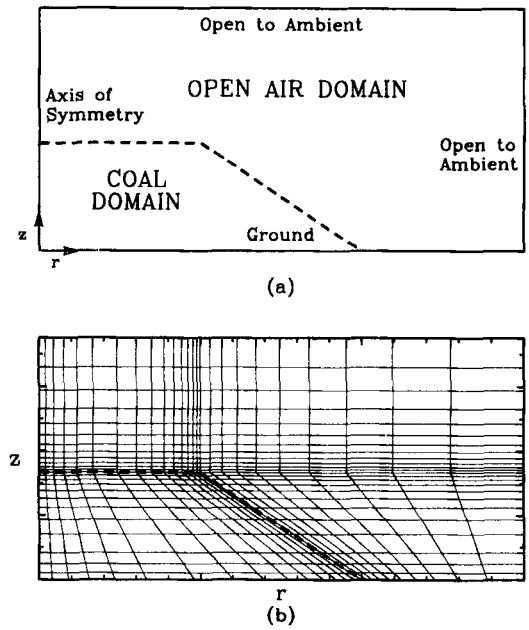

Figure 3. The coal stockpile ignition problem is used to study numerical formulations for a porous/open fluid system. (a) The axisymmetric domain includes the coal region and the surrounding air. (b) The mesh used for all calculations comprises 600 elements

reaction is occurring. Oxygen from the surrounding air enters the pile to fuel the reaction; the subsequent release of heat raises the temperature of the pile, which in turn drives buoyant flows within and outside the stockpile. We assume that the temperature, concentration, velocity and pressure fields are axisymmetric and solve for steady states of the system.

2.1. *Heat and mass transfer and chemical reaction*

Governing equations for heat and mass transfer through the system must account for the different thermophysical properties in each domain as well as the chemical reaction occurring in the coal stockpile. In the open fluid domain these equations take the non-dimensional forms

$$\mathbf{v} \cdot \nabla T = \frac{1}{Pr_o} \nabla^2 T, \tag{6}$$

$$\mathbf{v} \cdot \nabla C = \frac{1}{Sc_o} \nabla^2 C, \tag{7}$$

Within the coal stockpile

$$\mathbf{v} \cdot \nabla T = \frac{1}{Pr_p} \nabla^2 T + \beta Da C \exp\left(\gamma \frac{T}{1+T}\right), \tag{8}$$

$$\mathbf{v} \cdot \nabla C = \frac{1}{Sc_p} \nabla^2 C - Da C \exp\left(\gamma \frac{T}{1+T}\right). \tag{9}$$

In the above equations the dimensionless velocity is defined as $\mathbf{v} = \tilde{\mathbf{v}} \rho_{ref} L/\mu$, the dimensionless temperature is given by $T \equiv (\tilde{T} - \tilde{T}_{ref})/\tilde{T}_{ref}$ and the dimensionless oxygen concentration is denoted by $C \equiv \tilde{C}/\tilde{C}_{ref}$, where dimensional quantities are denoted by an overtilde and the subscript '*ref*' denotes reference or ambient conditions. All symbols are defined in the Appendix. The dimensionless Prandtl number Pr and Schmidt number Sc take different values in the open air and porous coal pile domains, as indicated by subscripts 'o' and 'p' respectively. These parameters, as well as the Prater number β, the Damkohler number Da and the Arrhenius number γ, are defined in Table I.

Table I. Definitions and values of dimensionless parameters used in calculations

Symbol	Description	Definition	Value
Da	Damkohler	$A\rho_{ref} L^2 e^{-\gamma}/\mu$	0·1*
Pr_o	Prandtl number for air in open fluid region	$\mu C_a/k_o$	0.72
Pr_p	Prandtl number for air in porous region	$\mu C_a/k_p$	0.09
Ra	Rayleigh number	$\rho_{ref}^2 C_a \beta_e \tilde{T}_{ref} g\beta/\mu k_p$	1×10^7
Sc_o	Schmidt number for air in open fluid region	$\mu/\rho_{ref}\mathscr{D}_o$	0.76
Sc_p	Schmidt number for air in porous region	$\mu/\rho_{ref}\mathscr{D}_p$	3.8
α	Slip coefficient	See equation (3)	1†
β	Prater number (adiabatic temperature rise)	$\tilde{C}_{ref}(-\Delta H)/\tilde{T}_{ref} C_a$	7.23
γ	Arrhenius number	$E/R\tilde{T}_{ref}$	23.3
η	Ratio of effective Brinkman and real viscosities	μ'/μ	1
λ	Dimensionless permeability	κ/L^2	$1{\cdot}2 \times 10^{-7}$

* Varied in bifurcation diagram calculations (Figures 4 and 9).
† Varied for calculations shown in Section 4.3.

Across the interface of the stockpile we specify continuity of the temperature and oxygen concentration and the heat and oxygen flux:

$$T_p = T_o, \tag{10}$$

$$\frac{1}{Pr_p}\mathbf{n}\cdot\nabla T_p = \frac{1}{Pr_o}\mathbf{n}\cdot\nabla T_o \tag{11}$$

$$C_p = C_o, \tag{12}$$

$$\frac{1}{Sc_p}\mathbf{n}\cdot\nabla C_p = \frac{1}{Sc_o}\mathbf{n}\cdot\nabla C_o, \tag{13}$$

where $\mathbf{n}$ denotes a unit vector normal to the surface of the coal pile.

Along the centreline and top of the open domain (see Figure 3(a)) no-flux conditions are set for heat and mass transfer. Along the ground the temperature is set to its ambient value and a no-flux condition is applied for oxygen transfer. Along the outer edge of the computational domain the temperature and concentration fields are set to ambient values.

2.2. Flow in the open domain and boundary conditions: Navier–Stokes equation

The flow in the open domain is governed by the steady state, Navier–Stokes equations, written here in dimensionless stress divergence form for an incompressible fluid with the Boussinesq approximation:[61]

$$\mathbf{v}\cdot\nabla\mathbf{v} = \nabla\cdot\sigma_o + \frac{Ra}{\beta Pr_p}T\mathbf{e}_z, \tag{14}$$

$$\nabla\cdot\mathbf{v} = 0, \tag{15}$$

where Ra is the dimensionless Rayleigh number (defined in Table I) and $\mathbf{e}_z$ is a unit vector oriented upwards against the direction of the gravitational force vector. The total stress tensor for a Newtonian fluid in the open fluid region, σ_o in equation (14), is given in dimensionless terms by

$$\sigma_o = -P\mathbf{I} + (\nabla\mathbf{v} + \nabla\mathbf{v}^T), \tag{16}$$

where the dimensionless dynamic pressure is defined as $P \equiv (\tilde{P} + \rho_{ref}gz)L^2\rho_{ref}/\mu^2$, $\mathbf{I}$ is the identity tensor and superscript T denotes the transpose operation.

The Navier–Stokes equations require the application of two distinct boundary conditions along all surfaces in this two-dimensional geometry. At the porous/open fluid interface we require continuity of normal stress:

$$\mathbf{n}\cdot\mathbf{n}\cdot\sigma_o = \mathbf{n}\cdot\mathbf{n}\cdot\sigma_p, \tag{17}$$

where σ denotes the total stress tensor for the fluid in each domain. The second boundary condition is a specification of the shear stress at the interface, $\mathbf{t}\cdot\mathbf{n}\cdot\sigma_o$, and depends on our choice of the flow equation in the porous region. The specific forms for this boundary condition and for σ_p will be presented in Sections 2.3.1 and 2.3.2.

To complete the specification of boundary conditions for the Navier–Stokes equations and the open fluid domain, the following choices are made. Stress-free boundary conditions are

imposed along the outer and upper surfaces of the computational domain. No-slip conditions are specified along the ground surface outside the coal pile and axisymmetry is enforced along the centreline in the open region.

2.3. *Flow in the porous domain and matching conditions*

2.3.1. The Darcy–slip formulation. If we choose to apply Darcy's law, equation (1), to describe buoyant flows within the porous medium, the dimensionless governing equations are as follows. We assume that the fluid is incompressible, apply the Boussinesq approximation[62,63] and express Darcy's law in stress divergence form to yield

$$-\nabla \cdot \boldsymbol{\sigma}_p = -\frac{1}{\lambda}\mathbf{v} + \frac{Ra}{\beta Pr_p} T\mathbf{e}_z, \tag{18}$$

$$\nabla \cdot \mathbf{v} = 0, \tag{19}$$

where λ is the dimensionless permeability (sometimes referred to as the Darcy number). The total stress tensor associated with Darcy's law is given by

$$\boldsymbol{\sigma}_p = -P\mathbf{I}. \tag{20}$$

This form is used to satisfy the normal stress continuity condition of equation (17). Note that the total stress tensor is isotropic, so the shear stress in a Darcy fluid is identically zero.

Only one boundary condition is needed for Darcy's law. This condition is chosen to require continuity of the flow normal to the boundary of the porous domain:

$$\mathbf{n} \cdot \mathbf{v}_p = \mathbf{n} \cdot \mathbf{v}_o. \tag{21}$$

For the second boundary condition for the Navier–Stokes equation one might be tempted to balance shear stresses tangential to the interface; however, this is not tenable, since, as discussed above, there are no shear stresses associated with Darcy's law. In reality the shearing force from the flow in the adjacent open region will be exerted on the fluid within the porous medium and on the solid porous structure itself. If the viscous shear force is not all transferred to the fluid in the porous region, it is reasonable to assume that the volume-averaged tangential velocity is discontinuous over the interface. This is the argument which leads to the slip condition originally put forth by Beavers and Joseph.[38]

When using Darcy's law, we employ a slip condition at the porous/open fluid interface for the shear stress boundary condition of the Navier–Stokes equation. Jones[44] extended the Beavers–Joseph condition to multidimensional flows by realizing the close relationship between the velocity derivative in equation (3) for unidirectional flow and the shear stress in the fluid of the open domain. The following dimensionless, vectorial form of Jones's modification to the Beavers–Joseph condition

$$\mathbf{t} \cdot \mathbf{n} \cdot \boldsymbol{\sigma}_o = \frac{\alpha}{\lambda^{1/2}} (\mathbf{t} \cdot \mathbf{v}_o - \mathbf{t} \cdot \mathbf{v}_p), \tag{22}$$

is applied at the interface between the coal pile and surrounding air in our Darcy–slip formulation. The quantity $\mathbf{t}$ in the above equation denotes a unit vector tangent to the porous/open fluid interface. No normal flow boundary conditions are applied at the remaining boundaries of the porous domain, namely the system centreline and the bottom of the coal pile.

2.3.2. The Brinkman formulation. The application of the Brinkman equation (2) to describe flows in the porous medium is straightforward. The dimensionless representation for an incompressible, Boussinesq fluid is given in stress divergence form by

$$-\nabla \cdot \boldsymbol{\sigma}_p = -\frac{1}{\lambda}\mathbf{v} + \frac{Ra}{\beta Pr_p} T\mathbf{e}_z, \tag{23}$$

$$\nabla \cdot \mathbf{v} = 0, \tag{24}$$

with the total stress tensor

$$\boldsymbol{\sigma}_p = -P\mathbf{I} + \eta(\nabla \mathbf{v} + \nabla \mathbf{v}^T), \tag{25}$$

where $\eta \equiv \mu'/\mu$ is the ratio of the effective viscosity of the Brinkman equation to that of the fluid in the open region. The stress tensor has the same form as that for the Newtonian fluid, equation (16), with the exception that the effective viscosity μ' multiplies gradients of velocity rather than the true fluid viscosity μ. This form of the total stress tensor is supplied to equation (17) for continuity of normal stress across the porous/open fluid interface.

The higher-order derivative of the velocity field in Brinkman's equation results in the need to specify two boundary conditions. These are supplied by matching normal and tangential velocities across the porous/open fluid interface:

$$\mathbf{n} \cdot \mathbf{v}_p = \mathbf{n} \cdot \mathbf{v}_o, \tag{26}$$

$$\mathbf{t} \cdot \mathbf{v}_p = \mathbf{t} \cdot \mathbf{v}_o. \tag{27}$$

When the Brinkman equation is used in the porous region, the secondary boundary condition for the Navier–Stokes equation requires the shear stresses to balance over the interface. It should be noted that the physical interpretation of this condition remains an open issue. For example, Nield and Bejan[64] argue that the integration of fluid stresses within the porous medium is over a smaller area at the porous/open interface than for the fluid in the open region, so a condition equating the stresses cannot be rigorously true. Nevertheless, we follow past convention and simply equate the fluid shear stresses at the interface:

$$\mathbf{t} \cdot \mathbf{n} \cdot \boldsymbol{\sigma}_o = \mathbf{t} \cdot \mathbf{n} \cdot \boldsymbol{\sigma}_p. \tag{28}$$

No-slip conditions are provided along the bottom of the coal pile and axisymmetry is imposed along the centreline.

3. NUMERICAL METHODOLOGY

We employ the Galerkin finite element method[65,66] to solve the system of partial differential equations resulting from each formulation. A finite element mesh consisting of quadrilateral elements is constructed over both porous and open domains, with elemental boundaries falling along the interface between the domains (see Figure 3(b)). Within each domain the appropriate governing equations are discretized and the proper boundary conditions are implemented.

In the following subsections we present an overview of our approach. For the sake of brevity we avoid an extended discussion of routine Galerkin finite element methodology and focus instead on the details involved with discretization of the Darcy and Brinkman equations and implementation of the matching conditions at the porous/open fluid interface.

3.1. *Discretization of the open domain equations*

In the open fluid region the temperature, concentration and velocity fields are approximated using expansions of nine-node biquadratic basis functions ϕ^i, while piecewise linear, discontinuous basis functions Γ^i (three per element) approximate the pressure:

$$\mathbf{v}(r, z) = \sum_{i=1}^{N_o} \begin{bmatrix} v_r^i \mathbf{e}_r \\ v_z^i \mathbf{e}_z \end{bmatrix} \phi^i(r, z), \tag{29}$$

$$\begin{bmatrix} T(r, z) \\ C(r, z) \end{bmatrix} = \sum_{i=1}^{N_o} \begin{bmatrix} T^i \\ C^i \end{bmatrix} \phi^i(r, z), \tag{30}$$

$$P(r, z) = \sum_{i=1}^{N_{o,P}} P^i \Gamma^i(r, z), \tag{31}$$

where v_r^i and v_z^i are the velocity unknowns, N_o is the number of nodes and $N_{o,P}$ is the number of pressure unknowns, all defined for the open fluid region. This mixed-order formulation (sometimes called the Q2P1 or 9/3 element[67]) has been demonstrated to be particularly efficient when used with the Galerkin finite element method to solve for incompressible flows.[68–70]

Galerkin's method is applied to the conservation equations (6) and (7) and the Navier–Stokes equations (14) and (15), which are integrated over the open fluid domain and weighted by multiplication by the appropriate basis function. Equations (6), (7) and (14) are then reduced to the weak form via integration by parts and the natural and essential boundary conditions along the top, outer, bottom and centreline of the open domain are implemented in the standard manner.[65,66]

The weighted residual of the momentum balance equation (14) in the open fluid region is given by the vector equation

$$\int_{D_o} \left(\nabla \mathbf{e}_k \phi^i : \boldsymbol{\sigma}_o - \mathbf{e}_k \phi^i \mathbf{v} : \nabla \mathbf{v} - (\mathbf{e}_k \phi^i \cdot \mathbf{e}_z) \frac{Ra}{\beta Pr_o} T \right) dV + \oint_{\partial D_o} \mathbf{e}_k \phi^i \mathbf{n} : \boldsymbol{\sigma}_o \, dS = 0, \tag{32}$$

where $k = r, z$. We will discuss the implementation of matching conditions along the surface of the porous medium for each formulation in the following subsections.

3.2. *Discretization of the porous domain equations*

In the porous coal region the temperature and concentration fields are approximated by biquadratic basis functions:

$$\begin{bmatrix} T(r, z) \\ C(r, z) \end{bmatrix} = \sum_{i=1}^{N_p} \begin{bmatrix} T^i \\ C^i \end{bmatrix} \phi^i(r, z), \tag{33}$$

where the coefficients T^i and C^i are mathematical unknowns for these expansions in the porous region and N_p is the total number of nodes in this region.

Analogously to the procedure discussed above, Galerkin's method is applied to the conservation equations (8) and (9), which are reduced to the weak form. The boundary conditions are implemented using standard finite element methodology.[65,66] Conveniently, the continuity conditions along the coal stockpile surface, equations (11)–(13), are naturally satisfied through the construction of the finite element basis functions and the weak form of the Galerkin weighted residuals.

The formulations for calculating flows through the porous medium and the implementation of matching conditions along the surface of the porous medium will be discussed in the following subsections.

3.2.1. The Darcy–slip formulation. We employ the following approach to solve Darcy's law within the porous medium. Since the continuity equation (19) is always solved in conjunction with the momentum balance equation (18), the two equations can be combined into a single equation for the pressure field:

$$\nabla \cdot \left(-\nabla P + \frac{\lambda Ra}{\beta Pr_p} T \mathbf{e}_z \right) = 0. \tag{34}$$

The velocity field within the porous medium is obtained by differentiating the pressure solution using the following derivation from equation (18):

$$\mathbf{v} = -\lambda \nabla P + \frac{\lambda Ra}{\beta Pr_p} T \mathbf{e}_z. \tag{35}$$

This type of formulation is commonly applied to describe flow through a saturated porous medium (see e.g. Reference 71); however, we believe that this is the first such application to coupled flows between a porous medium and an adjacent homogeneous fluid.

Interestingly, this approach may be superior to the mixed-order, primitive variable discretization owing to the inherent stability and convergence properties associated with the form of the finite element approximation to equation (34). While we present no direct evidence to support this contention here, it is consistent with our experiences in attempting to solve the coal stockpile ignition problem early-on, when a mixed-order discretization of velocity and pressure often yielded poor results (in terms of mass conservation difficulties and non-convergence with mesh discretization). There is also an interesting mathematical similarity between Darcy's law and the equations for inviscid, potential flow which supports the above hypothesis. For the case of an isothermal system with constant physical properties equation (34) simplifies to become Laplace's equation for the pressure, i.e. $\nabla^2 P = 0$; the description of potential flows can similarly be reduced to Laplace's equation for the potential. Lee *et al.*[72] employed the Galerkin finite element method to compute potential flows and found that solving the Laplace formulation with subsequent differentiation of the potential to yield the velocity field produced much more accurate results than use of a mixed method to directly solve for the velocity field. In fact, mixed formulations which performed well for viscous flows (such as the 9/3 element) were found to be very poor for inviscid flows. Consistent with these findings, it would not be surprising if the solution of equation (34) for the pressure field alone yielded better results than solution of the mixed-order, primitive variable discretization of Darcy's law.

Returning to implementation issues, the pressure field in the porous medium is expanded using biquadratic basis functions,

$$P(r, z) = \sum_{i=1}^{N_p} P^i \phi^i(r, z), \tag{36}$$

and the Galerkin weak form of equation (34) is formed. Green's theorem is applied to the entire equation, and the resulting expression in the surface integral is identified to be the fluid velocity from equation (35), to yield

$$\int_{D_p} \left(\nabla P \cdot \nabla \phi^i - \frac{Ra}{\beta Pr_p} T \frac{\mathrm{d}\phi^i}{\mathrm{d}z} \right) \mathrm{d}V + \oint_{\partial D_p} \mathbf{n} \cdot \mathbf{v}_p \phi^i \, \mathrm{d}S = 0. \tag{37}$$

Note that we have used equation (35) to write the surface integral of the above expression in terms of the velocity of the porous medium. This implementation simplifies the specification of boundary conditions for the pressure field within the porous medium, since they can be posed in terms of normal velocities along the domain surfaces. No-penetration boundary conditions, such as those applied along the system centreline and the ground, can be satisfied naturally by ignoring the surface integral in equation (37). Along the porous/open fluid interface the requirement of continuous normal flow between the regions, equation (21), is satisfied in the weak sense by substituting the normal velocity from the open region $\mathbf{n} \cdot \mathbf{v}_o$, into the surface integral of equation (37).

The remaining two interfacial boundary conditions, equations (17) and (22), are imposed through the surface integral of the Navier–Stokes residual, equation (32), in the following manner:

$$\int_{\partial D_{p,o}} \mathbf{e}_k \phi^i \mathbf{n} : \boldsymbol{\sigma}_o \, dS = \int_{\partial D_{p,o}} \left((\mathbf{e}_k \cdot \mathbf{n}) \cdot \boldsymbol{\sigma}_p + (\mathbf{e}_k \cdot \mathbf{t}) \frac{\alpha}{\lambda^{1/2}} (\mathbf{t} \cdot \mathbf{v}_o - \mathbf{t} \cdot \mathbf{v}_p) \right) \phi^i \, dS, \tag{38}$$

where $\partial D_{p,o}$ refers to the interface between the porous and open fluid domains, the subscript $k = r, z$, and $\boldsymbol{\sigma}_p$ is given by equation (20) which involves only the dynamic pressure within the porous medium.

3.2.2. The Brinkman formulation. For the Brinkman formulation we employ the same mixed-order representation of the velocity and pressure fields in the porous domain as that employed for the Navier–Stokes equations in the open fluid domain:

$$\mathbf{v}(r, z) = \sum_{i=1}^{N_p} \begin{bmatrix} v_r^i \mathbf{e}_r \\ v_z^i \mathbf{e}_z \end{bmatrix} \phi^i(r, z), \tag{39}$$

$$P(r, z) = \sum_{i=1}^{N_{p,P}} P^i \Gamma^i(r, z), \tag{40}$$

where N_p is the number of nodes and $N_{p,P}$ is the number of pressure unknowns in the porous domain. The Galerkin weak form of the Brinkman equation (23) is

$$\int_{D_p} \left(\nabla \mathbf{e}_k \phi^i : \boldsymbol{\sigma}_p + \frac{1}{\lambda} (\mathbf{e}_k \phi^i \cdot \mathbf{v}) - (\mathbf{e}_k \phi^i \cdot \mathbf{e}_z) \frac{Ra}{\beta Pr_p} T \right) dV + \oint_{\partial D_p} \mathbf{e}_k \phi^i \mathbf{n} : \boldsymbol{\sigma}_p \, dS = 0, \tag{41}$$

where $k = r, z$.

No-slip and axisymmetric boundary conditions are implemented along the coal pile bottom and centreline respectively using standard finite element methodology.[65,66] The continuity conditions of velocity and stress along the porous/open fluid interface, equations (17) and (26)–(28), are automatically satisfied by the continuity of the finite element basis and the additive cancelling of the boundary integrals arising from the weak form of the Galerkin weighted residuals, equation (32) and (41). The simplicity of this formulation makes the Brinkman formulation particularly attractive; in fact, only minor modifications are needed to convert existing Navier–Stokes codes to solve porous/open fluid problems (see e.g. Reference 73).

3.3. Solution of governing equations and parametric continuation

The finite element expansions are substituted into the Galerkin residual equations and nine-point Gaussian quadrature[74] is employed to convert the integral equations into a large set of non-linear algebraic equations. The Newton–Raphson method[74] is used to solve this system

iteratively and pseudo-arc-length continuation[75] is implemented to track the steady state solutions as a function of the Damkohler number. The resulting Jacobian matrix has an 'arrow' structure; it is banded except for the final row and column, which are full owing to components associated with the continuation routine. A direct solver written specifically for this type of matrix structure is used to solve the linear system.[76]

Figure 3(b) displays the finite element mesh used in all calculations performed here. This mesh consisted of 600 biquadratic elements and produced numerically convergent results for the Darcy–slip formulation under the conditions considered here, as verified in mesh resolution studies presented in Reference 77. The Darcy–slip formulation for this mesh resulted in a total of 10,592 mathematical degrees of freedom, while the Brinkman formulation on the same mesh produced 11,796 total unknowns. While the total number of unknowns was smaller for the Darcy–slip formulation owing to the pressure discretization discussed in Section 2.3.1, our numbering scheme resulted in a slight increase in the bandwidth of the Jacobian matrix. The Darcy–slip formulation required approximately 115 CPU seconds per Newton–Raphson iteration as compared with 150 CPU seconds per iteration for the Brinkman formulation on the Cray X-MP at the Minnesota Supercomputer Center. Each bifurcation diagram required 6–10 CPU hours.

4. RESULTS

We consider reaction, transport and flows within and around a porous coal stockpile which is shaped as a frustum sitting on the ground and surrounded by the atmosphere (see Figure 3(a)). The base of the coal pile has a dimensionless radius of unity, the dimensionless height of the pile is $\frac{1}{3}$, and the top of the coal pile has a dimensionless radius of $\frac{1}{2}$. The values of the parameters and dimensionless groups employed for this study are listed in Table I. Typical solutions to this problem are discussed in Section 4.1. A comparison between the Darcy and Brinkman formulations is presented in Section 4.2 and the effect of the value employed for the empirical Beavers–Joseph slip coefficient in the Darcy–slip formulation is examined in Section 4.3. A more comprehensive analysis of the ignition behaviour of coal stockpiles is presented in another paper.[18]

4.1. The coal stockpile ignition problem

We first present typical solutions to our model problem to set the stage for a critical examination of the different numerical formulations. Figure 4 shows a bifurcation diagram for the coal stockpile ignition problem where the maximum dimensionless temperature of the coal pile is plotted for each steady state solution as the Damkohler number Da is varied. The system exhibits multiple steady state solutions over a large range of Damkohler numbers, $10^{-3} \leq Da \leq 1$.

The S-shaped curves shown here are common for systems which display hysteresis phenomena and consist of three separate branches. The lower branch, near $T_{max} = 0$, consists of stable, extinguished steady states. This solution branch terminates at a turning point near $Da \approx 1$, which is termed the ignition point. The central section of the curve, where the slope is negative, represents temporally unstable steady state solutions. The upper branch is formed by stable, ignited solutions where reaction and transport rates are high enough to sustain vigorous combustion in the coal pile. The ignited branch is bounded by a turning point, termed the extinction point, at lower values of Damkohler number.

Typical features of steady states for this system are displayed in Figure 5, which shows

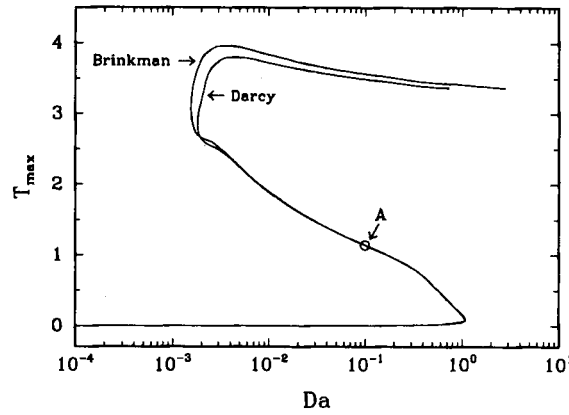

Figure 4. A bifurcation diagram plots the maximum temperature of steady state solutions versus the Damkohler number *Da* for both the Brinkman and Darcy formulations. Features of solutions at point A are shown in subsequent figures

streamfunction, temperature and concentration contours associated with a solution calculated with the Darcy–slip formulation; the solution corresponds to point A in Figure 4 and will be used to compare results from the two formulations in the next subsection. The streamlines indicate that fluid is flowing over and through the porous medium, with a strong plume rising from the top centre of the pile. The absolute magnitude of the streamfunction drops dramatically from the open fluid region to the interior of the coal stockpile, thus indicating much weaker flows within the porous medium. Smooth temperature and concentration contours within the porous region indicate that heat and mass transfer are dominated by diffusive phenomena within the coal pile. Distorted contours shaped by the buoyant plume above the pile show the importance of convective transport in the open fluid region.

4.2. A comparison of Brinkman and Darcy formulations

The bifurcation diagram discussed previously (Figure 4) shows curves obtained from both the Darcy and Brinkman formulations. Interestingly, although the positions of the ignited branches clearly differ, the formulations yield results which appear to be quite similar along the lower and middle branches of the diagram. However, a careful comparison of the predicted flows within the porous medium reveals significant differences between the two formulations.

We specifically examine the steady state solution denoted by point A in Figure 4. Two cuts through the model domain, indicated in Figure 6, will be employed to display radial and axial velocity profiles predicted by the different formulations in Figures 7 and 8. Note that for the Darcy formulation the fluid velocities are obtained by postprocessing the pressure and temperature fields in the porous medium via equation (35).

Figure 7 compares the radial velocity v_r plotted as a function of axial position for the two formulations. The Darcy–slip solution is smooth through the porous region; the circular symbol shows the discontinuity in tangential velocity at the surface of the pile which results from the Beavers–Joseph slip condition. The Brinkman solution oscillates from node to node within the porous medium; these oscillations are largest at the two surfaces of the coal pile, the ground at $z = 0$ and the porous/open fluid interface at $z = \frac{1}{3}$.

Figure 8 similarly shows axial velocity (v_z) profiles along a horizontal cut through the system. In Figure 8(a) the velocity scale is expanded to clearly show the solutions through the porous

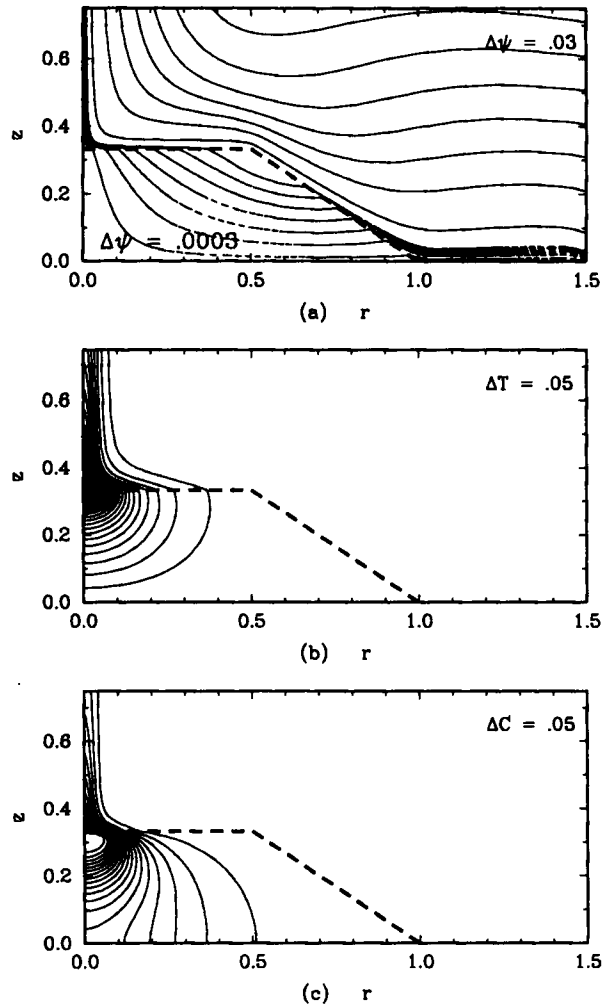

Figure 5. The dimensionless (a) streamfunction, (b) temperature and (c) concentration contours corresponding to point A on Figure 4 for the Darcy formulation. The contour spacings are indicated on each plot

medium. As in the radial velocity profiles shown previously, the Darcy–slip solution is smooth through the coal pile while the Brinkman solution exhibits node-to-node oscillations. The circles indicate the discontinuous tangential velocity at the porous/open fluid interface predicted by the Darcy–slip formulation and the cross marks the interfacial value of the continuous velocity predicted by the Brinkman formulation. Figure 8(b) plots the same velocity profiles and interface points on a scale to include the velocity in the open fluid region. Clearly the two implementation schemes yield similar results for the flow in the open fluid region.

4.3. Sensitivity to the slip coefficient

The Beavers–Joseph condition, equation (3), contains an empirical quantity, the slip coefficient α. While this quantity is postulated to depend only on the properties of the porous material, its value for any specific medium is not generally known and often must be determined from

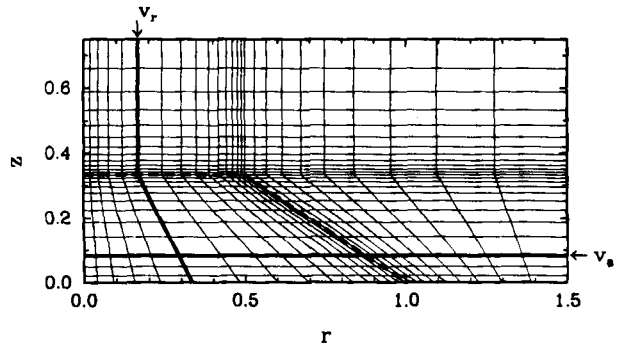

Figure 6. Bold lines show slices of domain along which one-dimensional velocity plots are compared in subsequent figures

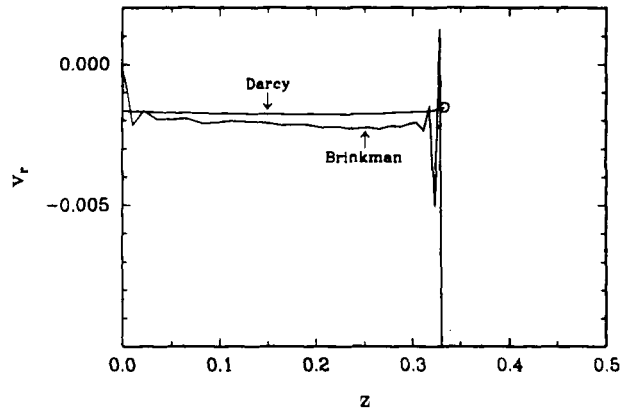

Figure 7. A comparison of radial velocity (v_r) profiles calculated from the Darcy and Brinkman formulations at conditions corresponding to point A on Figure 4. The porous/open fluid interface is located at $z = \frac{1}{3}$. The circle represents the discontinuity in the Darcy–slip solution

experiments. In all the calculations presented above a value of $\alpha = 1$ is employed, which is consistent with the derivation of Neale and Nader,[45] equation (4), and the choice of $\mu' = \mu$ for our calculations with the Brinkman formulation. The sensitivity of the Darcy–slip solutions to the value of α employed is explored by the calculations presented in this subsection.

Figure 9 shows parts of three bifurcation diagrams calculated with $\alpha = 0{\cdot}1$, 1 and 10. The three curves are nearly indistinguishable, so the ignition behaviour predicted by our coal stockpile model is not strongly affected by the value of the slip coefficient. Figures 10 and 11 show radial and axial velocity profiles along the cuts indicated in Figure 6 which were obtained using the three different values of α. Larger values of the slip coefficient result in greater discontinuities between the porous and open fluid velocities. However, the profiles do not change dramatically for the large variations in α considered here.

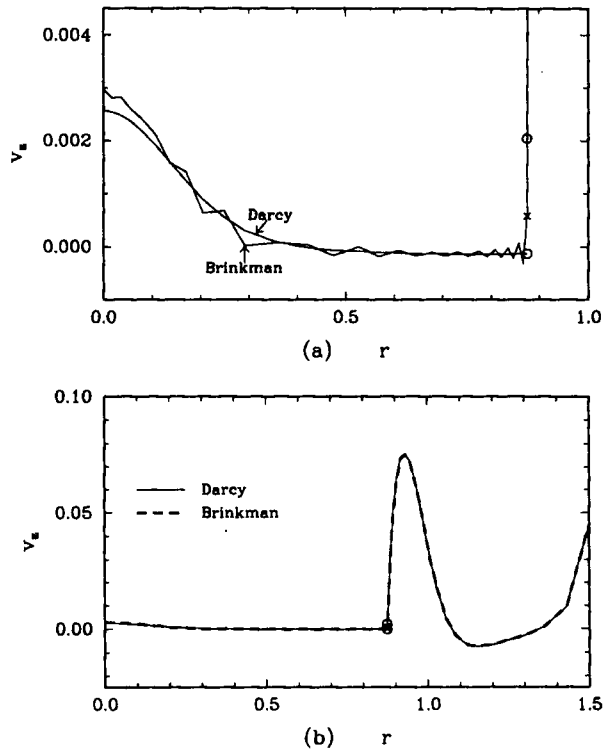

Figure 8. A comparison of axial velocity (v_z) profiles calculated from the Darcy and Brinkman formulations at point A on Figure 4: (a) magnification of porous region; (b) overall plot of the effect of the formulation on flow in the open fluid. The circle represents the jump in the Darcy solution; the cross is the interfacial value of the Brinkman solution

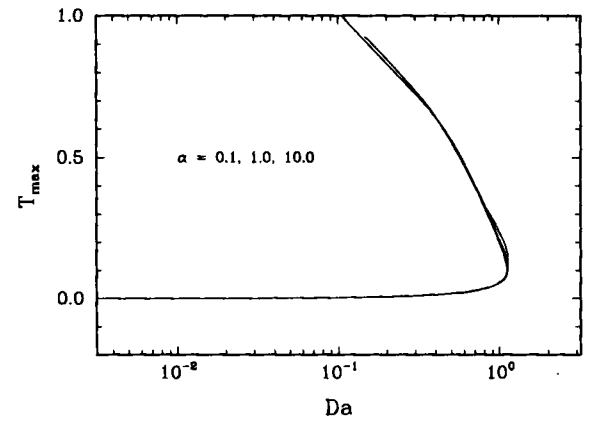

Figure 9. Bifurcation diagrams calculated for three values of the slip coefficient ($\alpha = 0{\cdot}1$, 1 and 10) show that the value of α has little overall effect on the ignition behaviour

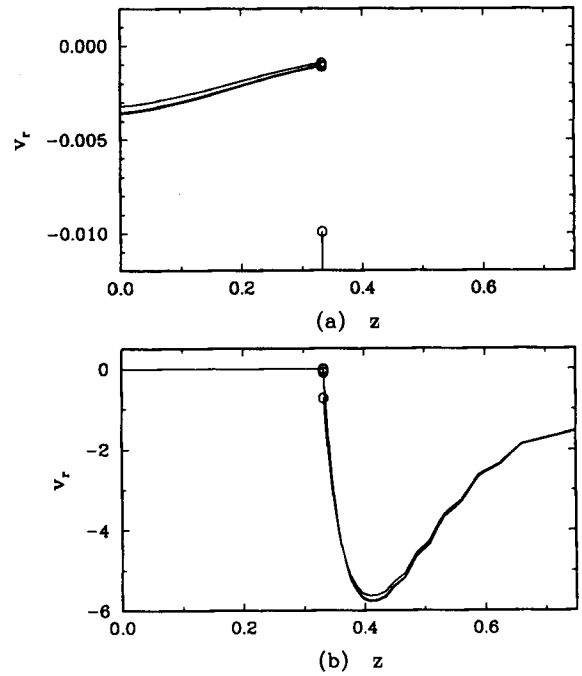

Figure 10. Comparison of radial velocity (v_r) profiles at the turning point in Figure 9 for three different values of the slip coefficient α: (a) magnification of porous region; (b) overall plot showing the effect of the slip coefficient on flow in the open fluid

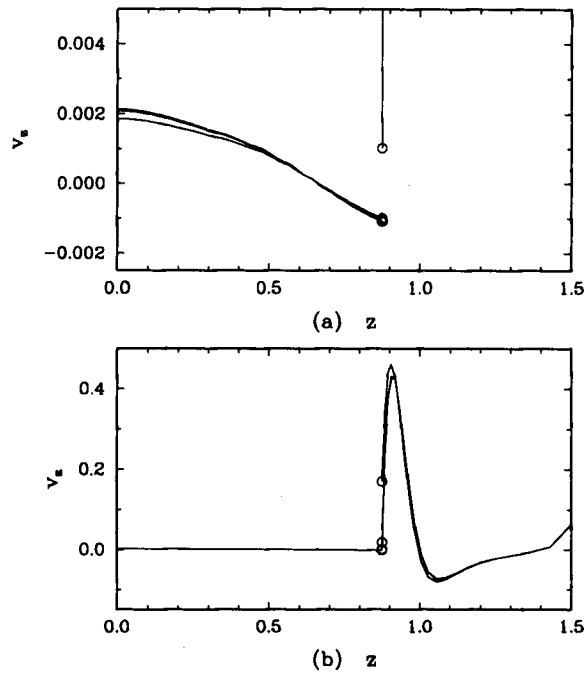

Figure 11. Comparison of axial velocity (v_z) profiles at the turning point in Figure 9 for three different values of the slip coefficient α: (a) magnification of porous region; (b) overall plot showing the effect of the slip coefficient on flow in the open fluid

5. CONCLUSIONS

Two different formulations which simultaneously resolve incompressible flows in a porous medium and a surrounding open fluid were applied to the coal stockpile ignition problem. Interestingly, the two curves in the bifurcation diagram of Figure 4 were very similar, indicating that the overall behaviour of the system was not strongly affected by the choice of formulation. This result is not surprising, since prior studies of this system[18] have shown that ignition–extinction phenomena are most strongly affected by convective transport through the open fluid region and diffusive transport within the porous medium rather than by flows within the coal pile.

The two formulations produced very different solutions for the velocity field within the porous medium. For calculations performed under identical conditions and on the same finite element mesh the Darcy–slip formulation yielded smooth solutions, while the Brinkman formulation produced a velocity field which contained significant oscillations throughout the porous domain. These oscillations or 'wiggles' are commonly observed in solutions to transport problems obtained using the Galerkin finite element method and broadcast a strong signal regarding the accuracy of the solution.[78] Since the objective of this study was to directly compare the performance of the two formulations under comparable discretizations, we did not pursue an extensive study of mesh resolution for the Brinkman solution. However, some comments on this issue may be useful. Several tests on meshes with more degrees of freedom indicated that mesh resolution for the Brinkman formulation tended to smooth the velocity profiles through the bulk of the porous region, yet the oscillations near the porous/open interface persisted for the several discretizations tested. This behaviour is consistent with our experience with other formulations for this problem (see the comments on use of a mixed-order discretization for Darcy's law in Section 3.2.1) and with the experience of other researchers who have employed the Brinkman formulation for porous/open fluid problems.[79] Certainly, elements adjacent to the interface must be small enough to resolve the porous boundary layer, whose thickness is $\mathcal{O}(\kappa^{1/2})$. Such an approach was used successfully by Nishimura *et al.*[56] Alternatively, numerical algorithms designed to damp such oscillations might be employed. The control volume scheme of Beckerman *et al.*[57] is an example of this approach. Gresho and Lee[78] warn, however, that techniques which *a priori* suppress wriggles must be used with great care to avoid inaccurate (but smooth) solutions on coarse meshes.

Each formulation presented certain advantages and disadvantages for solving the model problem considered here. The Darcy–slip formulation proved capable of yielding smooth solutions on a mesh which proved to be too coarse for the Brinkman formulation. Accurate solutions for the Darcy–slip formulation would likely be obtained with still coarser meshes than that employed here. For any given mesh size the Darcy–slip formulation will require fewer computational resources than the Brinkman formulation, since fewer mathematical degrees of freedom are needed. Our Darcy–slip implementation discretized only the pressure field in the porous medium rather than both the velocity and pressure fields as required by the Brinkman formulation. A potential disadvantage of the Darcy–slip formulation is the empiricism associated with the Beavers–Joseph condition; however, results of Section 4.3 demonstrated that the computations were relatively insensitive to the specific values employed for the slip coefficient.

The great advantage of the Brinkman formulation is the simplicity of its formulation and implementation, especially with regard to matching conditions between the porous and open fluid domains. However, this simplicity carries with it a significant computational burden to resolve the thin boundary layer at the surface of the porous medium. Indeed, this additional computational effort may not be justified in all situations, such as when the thickness of the porous boundary layer is much smaller than characteristic length scales of the system.

We advocate the use of the Darcy–slip formulation presented here for the solution of large-scale, coupled flows in porous and open fluid systems. While not as easily implemented as the Brinkman formulation, this approach proved superior in terms of solution accuracy, algorithmic robustness and computational costs.

ACKNOWLEDGEMENT

This work was supported in part by the University of Minnesota Army High Performance Computing Research Center (under the auspices of Army Research Office contract DAAL03-89-C-0038), the Minnesota Supercomputer Institute and the donors of the Petroleum Research Fund, administered by the American Chemical Society. A.G.S. would like to acknowledge support in the form of Graduate Fellowships from the National Science Foundation and the Army High Performance Computing Research Center; J.J.D. gratefully acknowledges the National Science Foundation for support through the PYI award program. P. M. Gresho of Lawrence Livermore National Laboratory, L. E. Scriven of the University of Minnesota and D. K. Gartling of Sandia National Laboratory provided useful insights to the authors about this work.

APPENDIX: NOMENCLATURE

A pre-exponential rate factor
C dimensionless concentration
C_a heat capacity of air
D mathematical domain volume
$\mathscr{D}$ diffusion coefficient
Da Damkohler number (see Table I)
D_p average particle diameter
$\mathbf{e}$ unit co-ordinate vector
E activation energy
$\mathbf{g}$ gravitational vector
h channel width in channel flow configuration (see Figure 1)
$\mathbf{I}$ identity tensor
k thermal conductivity
L characteristic length, chosen as radius of coal pile bottom
$\mathbf{n}$ unit normal vector
N number of degrees of freedom in finite element expansions
P dimensionless dynamic pressure
Pr Prandlt number (see Table I)
r dimensionless radial co-ordinate
R gas law constant
Ra Rayleigh number (see Table I)
Sc Schmidt number (see Table I)
$\mathbf{t}$ unit tangent vector
T dimensionless temperature
$\mathbf{v}$ dimensionless velocity
z dimensionless axial co-ordinate

Greek letters

α slip coefficient in Beavers–Joseph equation (3)
β Prater number (dimensionless adiabatic temperature rise) (see Table I)
β_e coefficient of thermal expansion
γ Arrhenius number (see Table I)
Γ piecewise discontinuous, linear basis functions
δ boundary layer thickness
ΔH heat of reaction
ε porosity of coal pile
η ratio of effective and true viscosities (see Table I)
κ permeability
λ dimensionless permeability (see Table I)
μ viscosity of air
μ' effective viscosity in porous medium, used in Brinkman equation (2)
ρ density of air
$\boldsymbol{\sigma}$ stress tensor
ϕ biquadratic basis functions
Ψ streamfunction

Mathematical symbols

∇ dimensionless gradient operator
$\cdot$ dot product
∂D boundary of domain D

Subscripts

o in the open fluid domain
p in the porous medium domain
r radial direction
ref at reference or ambient conditions
z axial direction

Superscripts

i numerical index
T transpose
$\sim$ dimensional quantity

REFERENCES

1. D. D. Joseph and L. N. Tao, 'Lubrication of a porous bearing—Stokes solution', *ASME J. Appl. Mech.*, **88**, 753–760 (1966).
2. C. C. Shir and D. D. Joseph, 'Lubrication of a porous bearing—Reynolds solution', *ASME J. Appl. Mech.*, **88**, 761–767 (1966).
3. B. C. Chandrasekhara, K. Rajani and N. Rudraiah, 'Effect of slip on porous-walled squeeze films in the presence of a magnetic field', *Appl. Sci. Res.*, **34**, 393–411 (1978).

4. E. M. Sparrow, J. W. Ramsey and R. G. Kemink, 'Freezing controlled by natural convection', *ASME J. Heat Transfer*, **101**, 578–584 (1979).
5. K. M. Fisher, 'The effects of fluid flow on solidification of industrial castings and ingots', *Phys. Chem. Hydrodyn.*, **2**, 311–326 (1981).
6. R. Viskanta, 'Mathematical modelling of transport processes during solidification of binary systems', *JSME Int. J. Ser. II*, **33**, 409–423 (1990).
7. V. R. Voller, 'An overview of the modelling of heat and fluid flow in solidification systems', in M. Rappaz, M. R. Ozgu and K. W. Mehin (eds), *Modeling of Casting, Welding, and Advanced Solidification Processes V*, The Metallurgical Society, Warrendale, PA, 1991, pp. 661–675.
8. T. Masuoka, 'Convective current in a horizontal layer divided by a permeable wall', *Bull. JSEM*, **17**, 225–237 (1974).
9. D. Poulikakos and M. Kazmierczak, 'Forced convection in a duct partially filled with a porous material', *ASME J. Heat Transfer*, **109**, 653–662 (1987).
10. H. T. Tang and Y. C. Fung, 'Fluid movement in a channel with permeable walls covered by porous media—a model of lung aveolar sheet', *ASME J. Appl. Mech.*, **97**, 45–50 (1975).
11. G. E. Barenblatt, I. P. Zheltov and I. N. Kochina, 'Basic concepts in the theory of homogeneous liquids in fissured rocks', *J. Appl. Math Mech.*, **24**, 1286–1303 (1960).
12. P. Cheng, 'Heat transfer in geothermal systems', in *Advances in Heat Transfer*, Vol. **14**, Academic, New York, 1978, pp. 1–105.
13. J. S. Y. Wang, C. F. Tsang and R. A. Sterbentz, 'The state of the art of numerical modelling of thermohydrologic flow in fractured rock masses', *Lawrence Livermore Berkeley Laboratory Rep. LBL-10524*, 1984.
14. F. A. Kulacki and G. Rajen, 'Buoyancy-induced flow and heat transfer in saturated fissured media', in S. Kakaç *et al.* (eds), *Convective Heat and Mass Transfer in Porous Media*, Kluwer, 1991, pp. 465–498.
15. C. L. Tien and J. T. Hong, 'Natural convection in porous media under non-Darcian and non-uniform permeability conditions', in S. Kakaç *et al.* (eds), *Natural Convection*, Hemisphere, Washington, DC, 1985.
16. N. Rudraiah, 'Flows past porous layers and their stability', in *Encyclopedia of Fluid Mechanics: Slurry Flow Technology*, Vol. 5, Gulf, Houston, TX, 1986.
17. V. Prasad, 'Convective flow interaction and heat transfer between fluid and porous layers', in S. Kakaç *et al.* (eds), *Convective Heat and Mass Transfer in Porous Media*, Kluwer, 1991, pp. 563–615.
18. A. G. Salinger, R. Aris and J. J. Derby, 'On modeling the spontaneous ignition of coal stockpiles', *AIChE J.*, in press.
19. H. P. G. Darcy, *Les Fontaines Publiques de la Ville de Dijon, Exposition et Application des Principes à Suivre et des Furmules à Employer dans les Questions de Distribution d'Eau*, Victor Dalmont, Paris, 1856.
20. H. C. Brinkman, 'A calculation of the viscous force exerted by a flowing fluid on a dense swarm of particles', *Appl. Sci. Res. A*, **1**, 27–34 (1947).
21. M. Muskat, *The Flow of Fluids through Porous Media*, McGraw-Hill, New York, 1937.
22. P. C. Carman, *Trans. Inst. Chem. Eng.*, **15**, 150 (1937).
23. M. Scheidegger, *The Physics of Flow through Porous Media*, MacMillan, New York, 1957.
24. S. Irmay, 'On the theoretical derivation of Darcy and Forchheimer formulas', *Trans. Am. Geophys. Un.*, **39**, 702–707 (1958).
25. Ph. Forchheimer, 'Wasserbewegung durch Boden. Z.', *Ver. Dt. Ing.*, **45**, 1781–1788 (1901).
26. S. Ergun, 'Fluid flow through packed columns', *Chem. Eng. Prog.*, **48**, 89–94 (1952).
27. K. Vafai and C. L. Tien, 'Boundary and inertia effects on flow and heat transfer in porous media', *Int. J. Heat Mass Transfer*, **24**, 195–203 (1981).
28. D. D. Joseph, D. A. Nield and G. Papanicolaou, 'Nonlinear equation governing flow in a saturated porous medium', *Water Resources Res.*, **18**, 1049–1052 (1982).
29. C. K. W. Tam, 'The drag on a cloud of spherical particles in low Reynolds number flow', *J. Fluid Mech.*, **38**, 537–546 (1969).
30. S. Childress, 'Viscous flow past a random array of spheres', *J. Chem. Phys.*, **56**, 2527 (1972).
31. T. S. Lundgren, 'Slow flow through stationary random beds and suspensions of spheres', *J. Fluid Mech.*, **51**, 273–299 (1972).
32. J. Koplik and H. Levine, 'Viscosity renormalization in the Brinkman equation', *Phys. Fluids*, **26**, 2864–2870 (1983).
33. S. Kim and W. B. Russel, 'Modelling of porous media by renormalization of the Stokes equations', *J. Fluid Mech.*, **154**, 269–286 (1985).
34. L. Durlofsky and J. F. Brady, 'Analysis of the Brinkman equation as a model for flow in porous media', *Phys. Fluids*, **30**, 3329–3341 (1987).
35. G. Neale, N. Epstein and W. Nader, 'Creeping flow relative to permeable spheres', *Chem. Eng. Sci.*, **28**, 1865–1874 (1973).
36. J. A. Kolodziej, 'Influence of the porosity of a porous medium on the effective viscosity in Brinkman's filtration equation', *Acta Mech.*, **75**, 241–254 (1988).
37. D. A. Nield, 'The boundary correction for the Rayleigh–Darcy problem, limitations of the Brinkman equation', *J. Fluid Mech.*, **128**, 37–46 (1983).
38. G. S. Beavers and D. D. Joseph, 'Boundary conditions at a naturally permeable wall', *J. Fluid Mech.*, **30**, 197–207 (1967).

39. G. S. Beavers, E. M. Sparrow and R. A. Magnuson, 'Experiments on coupled parallel flows in a channel and a bounding porous medium', *Trans. ASME, J. Basic Eng. D*, **92**, 843–848 (1970).
40. G. S. Beavers, E. M. Sparrow and B. A. Masha, 'Boundary condition at a porous surface which bounds a fluid flow', *AIChE J.*, **20**, 596–597 (1974).
41. G. Taylor, 'A model for the boundary condition of a porous material. Part 1', *J. Fluid Mech.*, **49**, 319–326 (1971).
42. S. Richardson, 'A model for the boundary condition of a porous material. Part 2', *J. Fluid Mech.*, **49**, 327–336 (1971).
43. P. G. Saffman, 'On the boundary condition at the surface of a porous medium', *Stud. Appl. Math.*, **L**, 93–101 (1971).
44. I. P. Jones, 'Low Reynolds number flow past a porous spherical shell', *Proc. Camb. Philos. Soc.*, **73**, 231–238 (1973).
45. G. H. Neale and W. K. Nader, 'Practical significance of Brinkman's extension of Darcy's law: coupled parallel flows within a channel and a bounding porous medium', *Can. J. Chem. Eng.*, **52**, 475–478 (1974).
46. S. M. Ross, 'Theoretical model of the boundary conditions at the fluid–porous interface', *AIChE J.*, **29**, 840–846 (1983).
47. N. Rudraiah, 'Coupled parallel flows in a channel and a bounding porous medium of finite thickness', *Trans. ASME*, **107**, 322–329 (1985).
48. C. L. M. H. Navier, *Mem. Acad. R. Sci. Inst. Fr.*, **6**, 389 (1827).
49. W. J. Silliman and L. E. Scriven, 'Separating flow near a static contact line: slip at a wall and shape of a free surface', *J. Comput. Phys.*, **34**, 287–313 (1980).
50. W. R. Schowalter, 'The behavior of complex fluids at solid boundaries', *J. Non-Newtonian Fluid Mech.*, **29**, 25–36 (1988).
51. G. H. Neale and W. K. Nader, 'Prediction of transport processes within the porous media: creeping flow relative to a fixed swarm of spherical particles', *AIChE J.*, **20**, 530–538 (1974).
52. D. A. Nield, 'Onset of convection in a fluid layer overlying a layer of a porous medium', *J. Fluid Mech.*, **81**, 513–522 (1977).
53. G. Pillatsis, M. E. Taslim and U. Narusawa, 'Thermal instability of a fluid-saturated porous medium bounded by thin fluid layers', *J. Heat Transfer*, **109**, 677–682 (1987).
54. M. E. Taslim and U. Narusawa, 'Thermal stability of horizontally superposed porous and fluid layers', *J. Heat Transfer*, **111**, 357–362 (1989).
55. C. W. Somerton and I. Catton, 'On the thermal instability of superposed fluid and porous layers', *Trans. ASME*, **104**, 160–165 (1982).
56. T. Nishimura, T. Takumi, M. Shiraishi, Y. Kawamura and H. Ozoe, 'Numerical analysis of natural convection in a rectangular enclosure horizontally divided into fluid and porous regions', *Int. J. Heat Mass Transfer*, **29**, 889–898 (1986).
57. C. Beckerman, S. Ramadhyani and R. Viskanta, 'Natural convection flow and heat transfer between a fluid layer and a porous layer inside a rectangular enclosure', in V. Prasad and N. A. Hussain (eds), *Natural Convection in Porous Media*, ASME, New York, 1986, pp. 1–12.
58. C. Beckerman, S. Ramadhyani and R. Viskanta, 'Natural convection flow and heat transfer between a fluid layer and a porous layer inside a rectangular enclosure', *J. Heat Transfer*, **109**, 363–370 (1987).
59. C. Beckerman, R. Viskanta and S. Ramadhyani, 'Natural convection in vertical enclosures containing simultaneously fluid and porous layers', *J. Fluid Mech.*, **186**, 257–284 (1988).
60. M. Song and R. Viskanta, 'Natural convection flow and heat transfer between a fluid layer and an anisotropic porous layer within a rectangular enclosure', in *Heat Transfer in Enclosures*, HTD Vol. 177, ASME, New York, 1991, pp. 1–12.
61. M. J. Boussinesq, *Theory Analytique de la Chaleur*, Vol. 2, Gauthier-Villars, Paris, 1903.
62. M. J. Boussinesq, 'Recherches théoriques sur l'écoulement des nappes d'eau infiltrées dan le sol et sur le débit des sources', *J. Math. (Paris)*, **10**, (1904).
63. D. K. Gartling and C. E. Hickox, 'A numerical study of the applicability of the Boussinesq approximation for a fluid-saturated porous medium', *Int. J. Numer. Methods Fluids*, **5**, 995–1013 (1985).
64. D. A. Nield and A. Bejan, *Convection in Porous Media*, Springer, New York, 1992.
65. G. Strang and G. J. Fix, *An Analysis of the Finite Element Method*. Prentice-Hall, Englewood Cliffs, NJ, 1973.
66. C. Johnson, *Numerical Solution of Partial Differential Equations by the Finite Element Methods*, Cambridge University Press, Cambridge, 1987.
67. P. M. Gresho, 'Contribution to Von Karman Institute lecture series on computational fluid dynamics: advection–diffusion and Navier–Stokes equations', *UCRL-92275*, Lawrence Livermore National Laboratory, Livermore, CA, 1985.
68. M. S. Engleman, R. L. Sani, P. M. Gresho and M. Bercovier, 'Consistent vs. reduced integration penalty methods for incompressible media using several old and new elements', *Int. J. Numer. Methods Fluids*, **2**, 25–42 (1982).
69. K. H. Winters, 'Laminar natural convection in a partially divided rectangular cavity at high Rayleigh number', *Int. J. Numer. Methods Fluids*, **8**, 247–281 (1988).
70. P. A. Sackinger, R. A. Brown and J. J. Derby, 'A finite element method for analysis of fluid flow, heat transfer and free interfaces in Czochralski crystal growth', *Int. J. Numer. Methods Fluids*, **9**, 453–492 (1989).
71. D. K. Gartling and C. E. Hickox, 'MARIAH—a finite element computer program for incompressible porous flow problems: theoretical background', *SAND79-1622*, Sandia National Laboratory, Albequerque, NM, 1982.

72. R. L. Lee, P. M. Gresho and R. L. Sani, 'An exploratory study on the application of an existing finite element Navier–Stokes code to compute potential flows', *UCRL-86684*, Lawrence Livermore National Labortaory, Livermore, CA, 1982.
73. M. S. Engleman, *FIDAP Users Manual, Revision 6.0*, Fluid Dynamics International, Inc., Evanston, IL, 1991.
74. G. Dahlquist and A. Björck, *Numerical Methods*, translated by N. Anderson, Prentice-Hall, Englewood Cliffs, NJ, 1974.
75. H. B. Keller, in P. H. Rabinowitz (ed.), *Applications of Bifurcation Theory*, Academic, New York, 1977, p. 359.
76. P. D. Thomas and R. A. Brown, 'LU decomposition of banded matrices with augmented dense constraints', *Int. J. Numer. Methods Eng.*, **24**, 1451–1459 (1986).
77. A. G. Salinger, 'The interactions of transport mechanisms in convecting and reacting systems', *Ph.D. Thesis*, Department of Chemical Engineering and Materials Science, University of Minnesota, Minneapolis, MN, 1993.
78. P. M. Gresho and R. L. Lee, 'Don't suppress the wiggles— they're telling you something', *Comput. Fluids*, **9**, 223–253 (1981).
79. D. K. Gartling, personal communication, 1993.